8. Modeling *FIRAS* Spectra

There are four known astrophysical contributors to the *FIRAS* spectra: the cosmic microwave background radiation (CMBR), thermal Galactic dust emission, narrow atomic and molecular lines from interstellar gas, and solar system thermal dust emission (zodiacal emission). The determination of these components is the subject of a number of papers from the *FIRAS* analysis team (Section 8.2 and Appendices A and D). The project data sets include a determination of the contributors' intensities and properties, though there may be slight differences in the techniques used from those of the refereed published results, which should be considered definitive. In this section we discuss how the delivered products were produced. They can be duplicated using the delivered material. Except where explicitly stated otherwise the delivered products' production did not include the appropriate "off-diagonal" weights for the pixel-pixel and frequency-frequency correlations. The derived uncertainties can be much smaller than what the more detailed analysis would derive.

The delivered products were based on a four part analysis of the combined HIGH and LOWF data sets: (1) A model, provided by the *COBE DIRBE* analysis team, for zodiacal emission was subtracted from the HIGH; (2) A model CMBR (monopole and dipole) was fit to the LOWF data, and then subtracted from both the LOWF and HIGH data; (3) A model galaxy was fit to the LOWF and HIGH data and subtracted; (4) The residual was fit to a polynomial baseline and line profiles to determine the line intensity maps.

8.1. Zodiacal Emission Model

The zodiacal emssion is thermal emission from dust, with temperatures of order 250 K, that is in a cloud generally centered on the sun. There are strong variations in the dust quantity and temperature as a function of distance to the sun, and the projected distance out of the ecliptic plane. The peak of the emission is at frequencies higher than covered by *FIRAS* though its low frequency tail can impact the *FIRAS* data, particularly for $\nu > 20$ cm^{-1}, attaining intensities comparable to the galactic dust emission at 100 cm^{-1} for the lowest intensity pixels.

The existence of zodiacal emission can be confirmed with the *FIRAS* data, but they lack the signal to noise to be able model the emission in detail. For that we have relied on a model derived by the *COBE DIRBE* team based on a parametric fit of a geometric model to the time variation in their data. The particular model and parameters used (*DIRBE* Science Pipeline Run 6) are to be described in detail by Kelsall *et al.* (1998).

The *DIRBE* zodiacal emission model is explicitly calculated only for the particular *DIRBE* band wavelengths. The most relevant ones for the *FIRAS* are the two longest wavelength *DIRBE* bands at 1260 and 2128 GHz (240 and 140 μm). The *DIRBE* model was interpolated/extrapolated to the entire *FIRAS* band by fitting a power law emissivity that connected the two *DIRBE* points.

This *DIRBE* based model can be compared in detail to the *FIRAS* sky, at least at the lower flux levels seen outside the galactic plane. Though the *FIRAS* data set is itself insufficient to derive the the details of the zodiacal model, it can constrain the general normalization and the emissivity power law index. Earlier versions of the *DIRBE* model were clearly improved if the emissivity was steepened, and the overall intensity reduced for the *FIRAS* frequencies. These changes were clearly important in that they could induce systematic shifts in the determined galactic dust properties by as much as 5% in temperature and 25% in amplitude.

In addition to its use in the astrophysical fits of the *FIRAS* spectra, the zodiacal model was used by the destriper (Section 6.5). The destriper depends on the constancy of all the spectra within a pixel. Temporal variations are induced in the spectra as the earth moves through the zodiacal dust cloud. For this purpose the unadjusted *DIRBE* model was used to calculate the expected *FIRAS* emission as a function of time for each coadd. The destriper runs for the high frequency channels then subtracted these spectra before the destriping. After the stripe amplitudes were determined, and the destriped pixel spectra calculated, the zodiacal model intensities were then added back to the pixel spectra so that the project data sets *still contain the entire contribution from zodiacal emission.*

For the analysis data sets, whose production are described in the following sections (8.2–8.4), the *DIRBE* based zodiacal emission model, without alteration, was first subtracted from the HIGH spectra.

8.2. CMBR Determination

8.2.1. Temperature Maps

The low-frequency spectra (LOWF) are dominated by the cosmic background, but they contain a significant Galactic spectral component which must be well-modeled in order to derive accurate CMBR temperatures. We do so by computing an empirical Galactic spectrum at each frequency by modeling the sky with three spatial templates: a uniform component, a dipolar (Doppler-shifted) component, and a Galactic component that we assume correlates spatially with the average high-frequency intensity at each pixel. That is

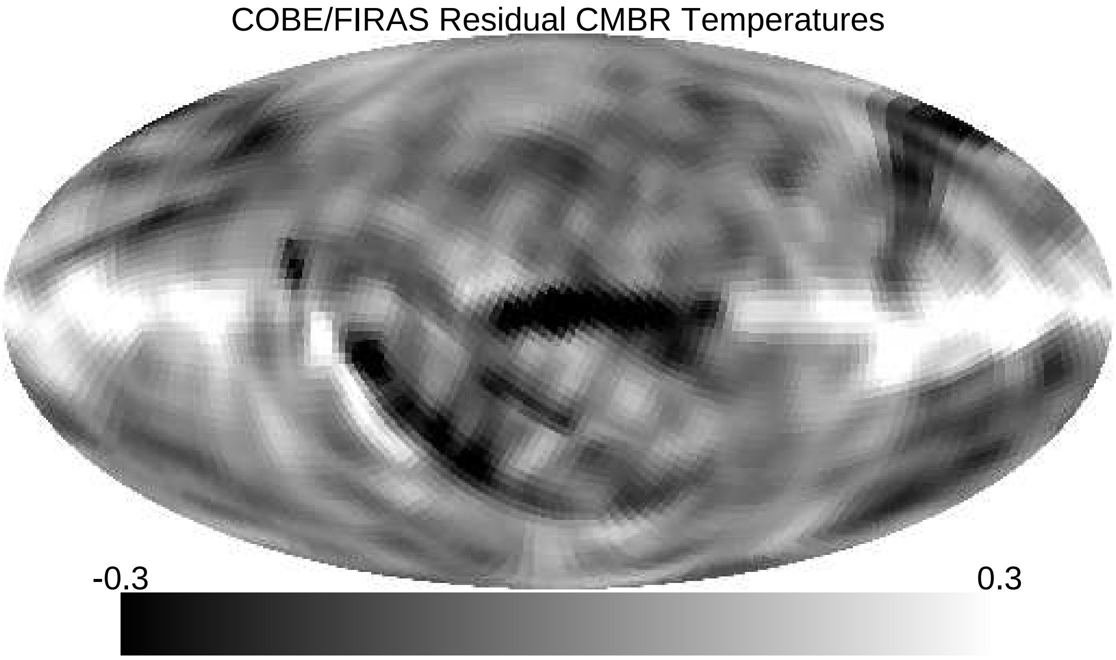

Fig. 8.1.— CMBR residual temperature — (mK). Both the monopole and dipole terms have been removed. This and all other maps in the explanatory supplement have been projected in Galactic coordinates. In addition, a color postscript version of this and all other maps are available, see Appendix K.

we minimize:

$$\chi^2_\nu = \sum_p \left[S_{p\nu} - u_\nu - D^x_p d^x_\nu - D^y_p d^y_\nu - D^z_p d^z_\nu - G_p g_\nu\right]^2 n_p \tag{36}$$

where

$$D^x_p \equiv \cos(b_p)\cos(l_p),\ \ D^y_p \equiv \cos(b_p)\sin(l_p),\ \ D^z_p \equiv \sin(b_p) \tag{37}$$

provide the dipole spatial pattern based on the pixel position (l_p, b_p), and G_p is the weighted average of the combined high-frequency skymap for frequencies above 25 cm^{-1} and n_p is the pixel weight. Pixels within 15° of the Galactic plane are excluded from the fit. The derived Galactic spectrum, g_ν, is next used to compute the CMBR temperature using the model:

$$\chi^2_p = \sum_\nu \left[S_{p\nu} - P(\nu; T_0) - \Delta T_p \frac{\partial P(\nu; T_0)}{\partial T} - G_p g_\nu\right]^2 \frac{n_p}{C^2_\nu} \tag{38}$$

where $P(\nu; T_0)$ is a Planck spectrum at $T_0 \equiv 2.728°$, ΔT_p are the temperature corrections and we fit a new value for G_p, the "amount" of Galaxy in each pixel. The fractional expression at the end gives the spectral weight at each frequency. The final CMBR temperatures are given by:

$$T_p = 2.728° + \Delta T_p. \tag{39}$$

These temperatures are computed at each pixel for the low frequency destriped skymap. We can compute an overall CMBR temperature and dipole temperature (amplitude) and direction by spatially decomposing the temperature map much as before. That is:

$$T_p \ = \ T_{cmbr} \ + \ D^x_p\, T_x + D^y_p\, T_y + D^z_p\, T_z \tag{40}$$

where T_{cmbr} is the CMBR temperature and T_x, T_y, T_z are the dipole temperature components from which we compute the dipole amplitude and direction.

The CMBR temperature and the CMBR residual temperature for each pixel in the input skymaps make up the CMBR analyzed science data set. The FITS header for the *FIRAS* CMBR temperature map is given in Appendix G.

Figure 8.1 is a map of the CMBR residual temperature projected in Galactic coordinates. Residual effects of 0.5 - 1.0 mK can be seen in the Galactic plane. Otherwise, the map is free of obvious systematic effects, and is roughly consistent with a normal distribution with an RMS scatter of 214 μK for Galactic latitudes greater than 15°. The uncertainty in the CMBR temperature for any given pixel is dominated by the detector noise and *PUP* uncertainty.

We have performed an autocorrelation analysis of the CMBR temperature residuals as a function of angular separation. The results are consistent with the *DMR* anisotropy results (Fixsen *et al.*, 1997a) .

8.2.2. Considerations When Modeling Cosmological Parameters

The cosmic background as measured by *FIRAS* is very well described by a Planck spectrum, therefore in order to detect any significant deviation from this, it is necessary to compute a full-sky average to obtain sufficient signal to noise. We calculate this spectrum, along with the CMBR dipole and "average" Galactic spectrum by finding the "projections" of the sky along three spatial templates. The first two are a uniform template with value one everywhere and a dipole template, $\cos(\theta)$, where θ is the angle between the given pixel and the dipole direction. The Galactic template is more problematical but is approximated with an average Galactic intensity derived from the high frequency channels (cf. section 8.2.1). To derive the spectra we minimize:

$$\chi^2_\nu \; = \; \sum_{pp'} [(S_{p\nu} - u_\nu - D_p d_\nu - G_p g_\nu) W_{pp'} (S_{p'\nu} - u_\nu - D_{p'} d_\nu - G_{p'} g_\nu)]^2 \qquad (41)$$

with respect to u_ν, d_ν, and g_ν where D_p and G_p are the dipole and Galactic templates and $w_{pp'}$ are the pixel weights described in the previous section, with the sums performed over the relevant pixels. Here we explicitly include the pixel-pixel correlations. The spectra are computed frequency by frequency.

The amount of non-thermal distortion in the CMBR is generally shown by the residuals of a fit of u_ν to a Planck spectrum, $P(\nu;T)$. The parameters of specific cosmological models are fit directly in equation 41, expanded to include a $\Sigma_{\nu\nu'} w_{\nu\nu'}$ weighted sum over frequency. Alternatively we fit a model to the u_ν derived from the general fit of equation 41. Examples of the cosmological models used are: a Bose-Einstein spectrum to compute μ, the chemical potential; or a Planck plus Zel'dovich-Sunyaev spectrum to compute y, the Comptonization (Kompaneets) parameter. The cosmic background temperature, T_{cmbr}, is computed. The two models are given by:

$$M(\nu, T_{cmbr}, \mu) \; = \; \frac{2hc^2\nu^3}{\exp(x+\mu) - 1} \qquad (42)$$

and

$$M(\nu, T_{cmbr}, y) \; = \; P(\nu, T_{cmbr}) \, + \, T_{cmbr} \left[\frac{x(1+\exp(-x))}{1-\exp(-x)} - 4 \right] \frac{\partial B}{\partial T} y \qquad (43)$$

respectively, where $x \equiv hc\nu/kT$. In fits of u_ν the effective weight must include its statistical uncertainty, which including the frequency dependent weights is:

$$w_{u;\nu\nu'} \;=\; w_{\nu\nu'} \sum_{pp'} w_{pp'} C_\nu^2. \tag{44}$$

The small allowed level of distortion generally assures that the model can be linearized in terms of the parameters, maintaining the linear nature of the problem. Although this fit is not technically difficult, it demands care to ensure that all systematic errors are properly accounted for. For example, some "Galactic" signature "leaks" in to the uniform spectrum, so it is usually necessary to include a supplementary Galactic spectrum in the fit along with the cosmological models (cf. equation 38). It is necessary to consider the sensitivity of the parameter values to Galactic latitude cutoff.

8.3. Galactic Dust Parameter Maps

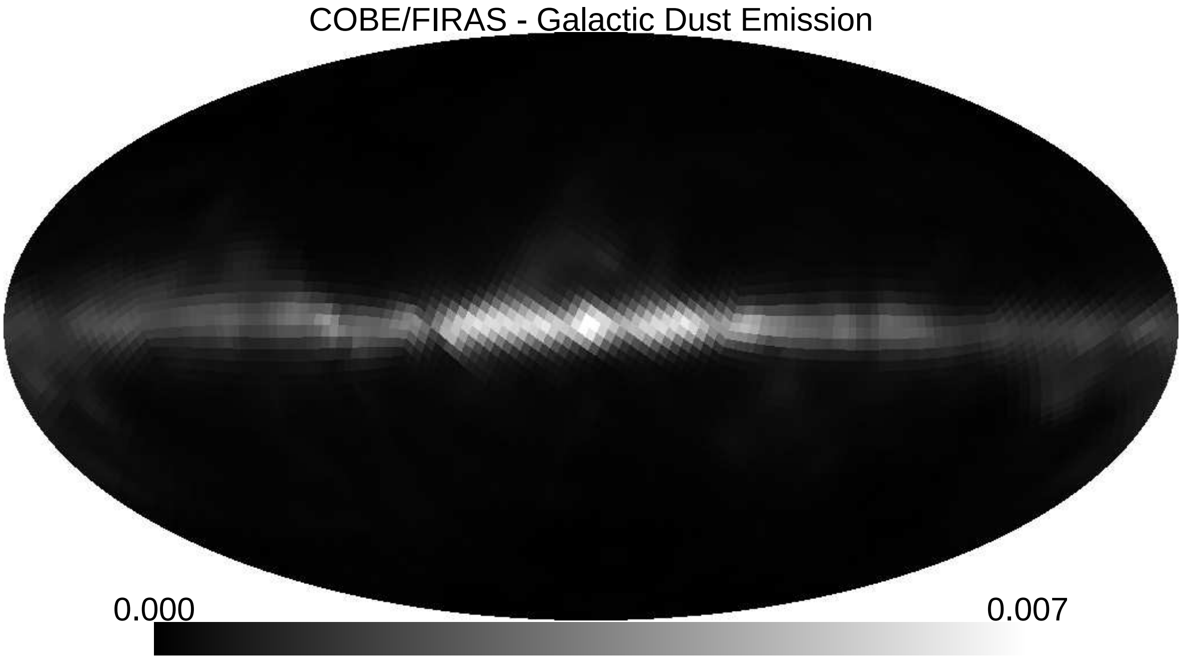

Fig. 8.2.— Galactic dust emission — τ. See equation 45, $\nu_0 = 1800$ GHz. (qv. Figure 8.4)

We use the map of CMBR temperatures derived above to subtract the CMBR, $P(\nu, T_{\mathrm{cmbr};p})$ from both the LOWF and HIGH spectra. As we have already removed the

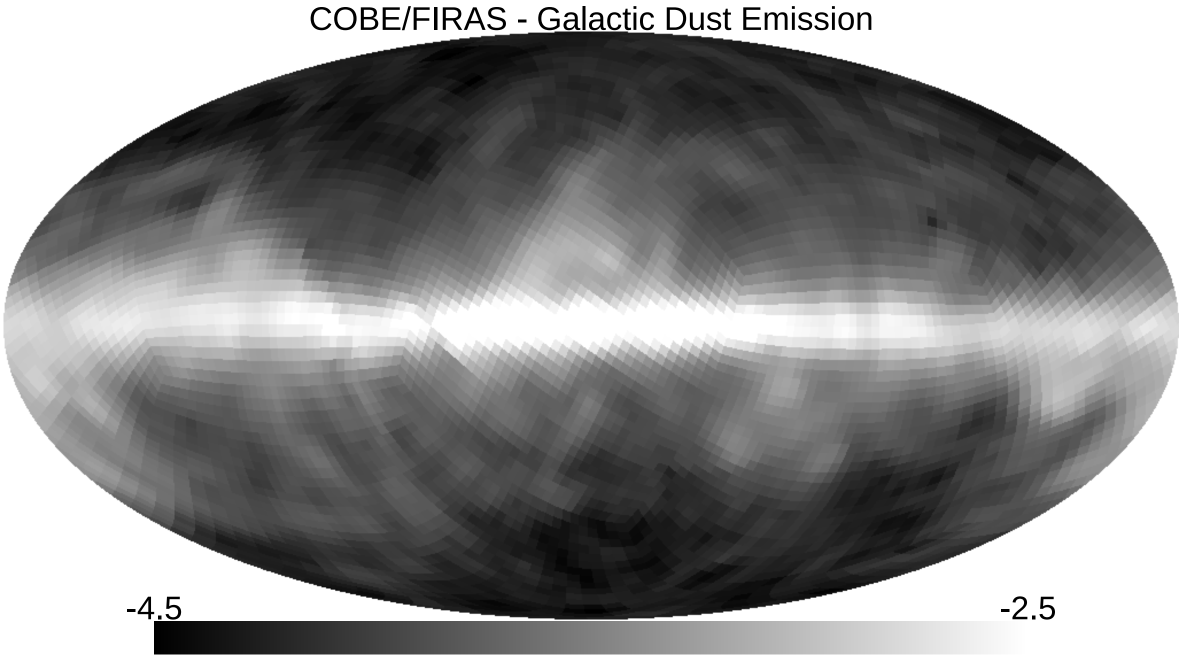

Fig. 8.3.— Galactic dust emission, logarithmic stretch — (qv. Figure 8.2)

zodiacal emission, the remaining signal is expected to be a continuum from galactic dust; narrow lines from the interstellar gas; and some possible contribution from an extragalactic "far infrared background" (FIRB). We made no explicit allowance for a FIRB in the delivered analysis data sets. (For a discussion of the FIRB and *FIRAS* data see Shafer *et al.* 1998ab; Fixsen *et al.* 1998; Hauser *et al.* 1998). The galactic dust is well characterized by a modified Planck spectrum:

$$M_{\nu p} \; = \; \tau_p \left(\frac{\nu}{\nu_0}\right)^{\alpha_p} P(\nu, T_{\mathrm{dust};p}). \tag{45}$$

The value of τ_p is a measure of the relative dust column for each pixel, though its numerical value depends on the value used for the scaling frequency, ν_0, which we have set to 1800 GHz. The galactic spectral form is not uniform over the entire sky, which can be modeled with pixel to pixel variations in temperature, $T_{\mathrm{dust};p}$, and/or emissivity index, α_p (Reach *et al.* 1995). At higher galactic latitudes, the signal to noise is inadequate to fit both parameters, though if α is held at a fixed value for most pixels a moderately precise number for $T_{\mathrm{dust};p}$ is derived, within a few Kelvin.

The delivered analysis data sets include a pixel by pixel fit of the dust properties. For the LOWF we only determined the dust column, τ_p, fixing the temperature at 18° K. For the

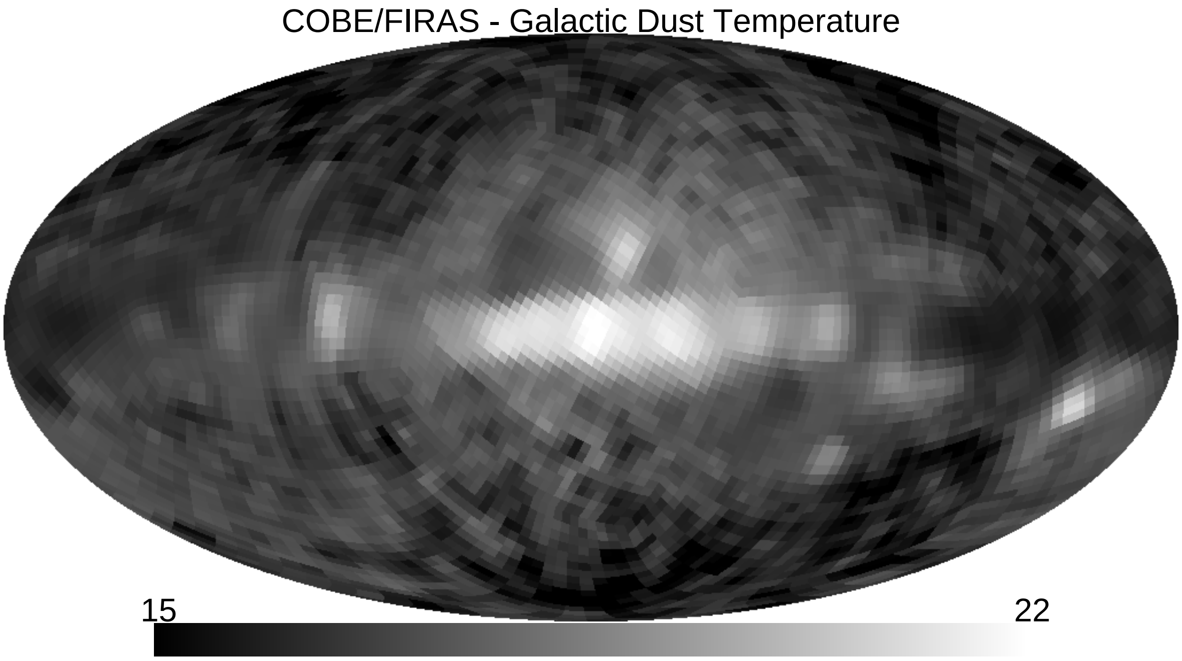

Fig. 8.4.— Galactic dust temperature — (K). From a single temperature model fit, with no removal of any isotropic far infrared cosmic background. It should be regarded as illustrative. (qv. Figure 8.1)

HIGH frequencies we fit both $T_{\mathrm{dust};p}$ and τ_p. The emissivity index was fixed at $\alpha = 2$, which was determined by a fit to the average high galactic latitude ($|b| > 20°$) spectrum. The fits did not include the frequency to frequency covariance. The delivered uncertainties include only the contribution from the detector noise. Near the Galactic plane the *FIRAS* gain uncertainties are significant.

8.4. Spectral Lines

In the *FIRAS* frequency range there are a number of narrow molecular and forbidden atomic lines produced by the interstellar gas (Table 8.1, Wright *et al.* 1991; Bennett *et al.* 1994). The *FIRAS* instrumental resolution is large compared to the expected width of the features so that they can be treated as delta function sources. Using a model for the instrument, we have produced synthetic profiles of the lines' expected contribution to the *FIRAS* spectra. These profiles, besides illustrating the intrinsic resolution of the instrument, are used in determining the intensity and significance of the line. A set of these profiles is included with the project data sets (Table 8.1).

8.4.1. Generating Line Profiles

The line profile model assumes that the interferogram of each line is a simple cosine subject to self-apodization arising from beam divergence effects. For data near the galactic center, the intensity of the 157.7 μm [C II] and 205 μm [N II] lines was so high that their signal was visible in the interferogram (as the sum of two cosines) over most of the short stroke interferogram. The self-apodization was observed in the modulation of the cosine amplitudes versus path difference. This showed that for the [C II] line, the self apodization is best described by a Gaussian with a width of 156 sample points. The [N II] line was similarly apodized with a width that scaled inversely with the line frequency. The model line interferogram is:

$$I(x) \; = \; \cos(2\pi\nu_L x) \, \exp[-\frac{1}{2}(\frac{\nu_L}{\nu_\circ}\frac{x}{\sigma})^2] \qquad (46)$$

where x is the optical path difference, ν_L is the line frequency, $\nu_\circ$ is the Nyquist frequency of the instrument, and $\sigma = 5.37$ mm is the width of the Gaussian self-apodization function.

The synthetic interferogram is processed in a manner similar to that used to generate sky spectra from coadded IFGs. The interferogram is further apodized with the apodization function described in Section 5.1, then Fourier transformed to produce a synthetic single-line spectrum for an ideal instrument. At this point, the processing of the synthetic

Table 8.1: Spectral Lines Fit in *FIRAS* Data

Species	ν (cm^{-1})	ν (GHz)	λ (μm)	Excluded Frequencies‡ (cm^{-1})
CO (J=1-0)*	3.845	115.27	2600.7	–
CO (J=2-1)	7.690	230.54	1300.4	–
CO (J=3-2)	11.535	345.80	867.0	–
O_2*	14.168	424.75	705.8	–
CO (J=4-3)	15.378	461.04	650.3	–
[C I]	16.419	492.23	609.1	–
H_2O*	18.576	556.89	538.3	–
CO (J=5-4)	19.222	576.27	520.2	–
CO (J=6-5)	23.065	691.47	433.6	22.9–23.4
CO (J=7-6)**	26.908	806.68	371.6	26.5–27.5
[C I]**	27.00	809.44	370.4	
H_2O†	37.136	1113.3	269.3	36.5–37.4
[N II]	48.738	1461.1	205.2	47.5–49.2
H_2O (J=2-1)*	57.26	1716.6	174.6	–
[C II]	63.395	1900.5	157.7	62.8–64.2
[O I]	68.716	2060.1	145.5	68.3–69.2
[Si I]*	77.11	2311.7	129.7	76.9–77.4
[N II]	82.036	2459.4	121.9	81.9–82.4
CH (J=2-1)	86.38	2589.6	115.77	–

*Only upper limits determined.

**Only a single line profile with $\nu = 27 cm^{-1}$is in the delivered data sets.

†Observed in absorption.

‡Frequencies (cm^{-1}) removed during continuum thermal dust spectral fits.

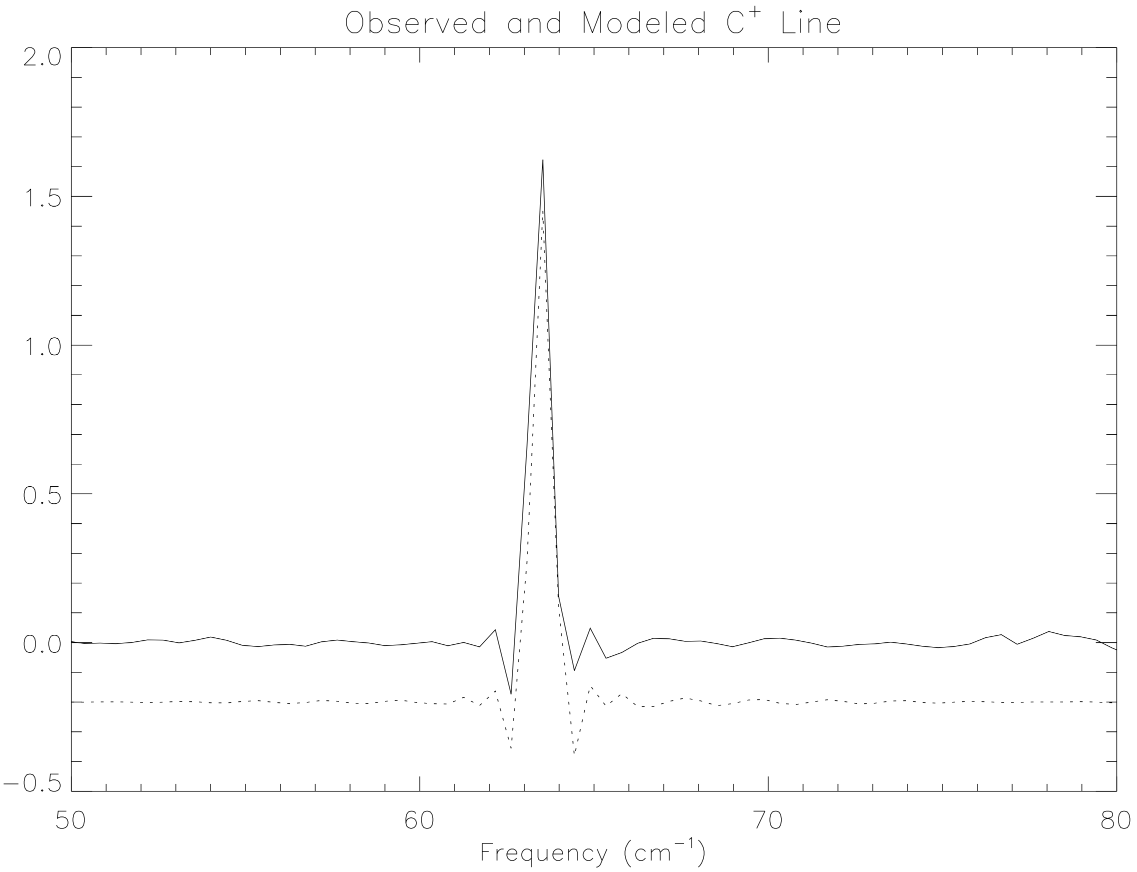

Fig. 8.5.— Observed and model [CII] line profiles — The shape of the modeled [CII] line (dotted) matches the observed (solid) shape of the [CII] line.

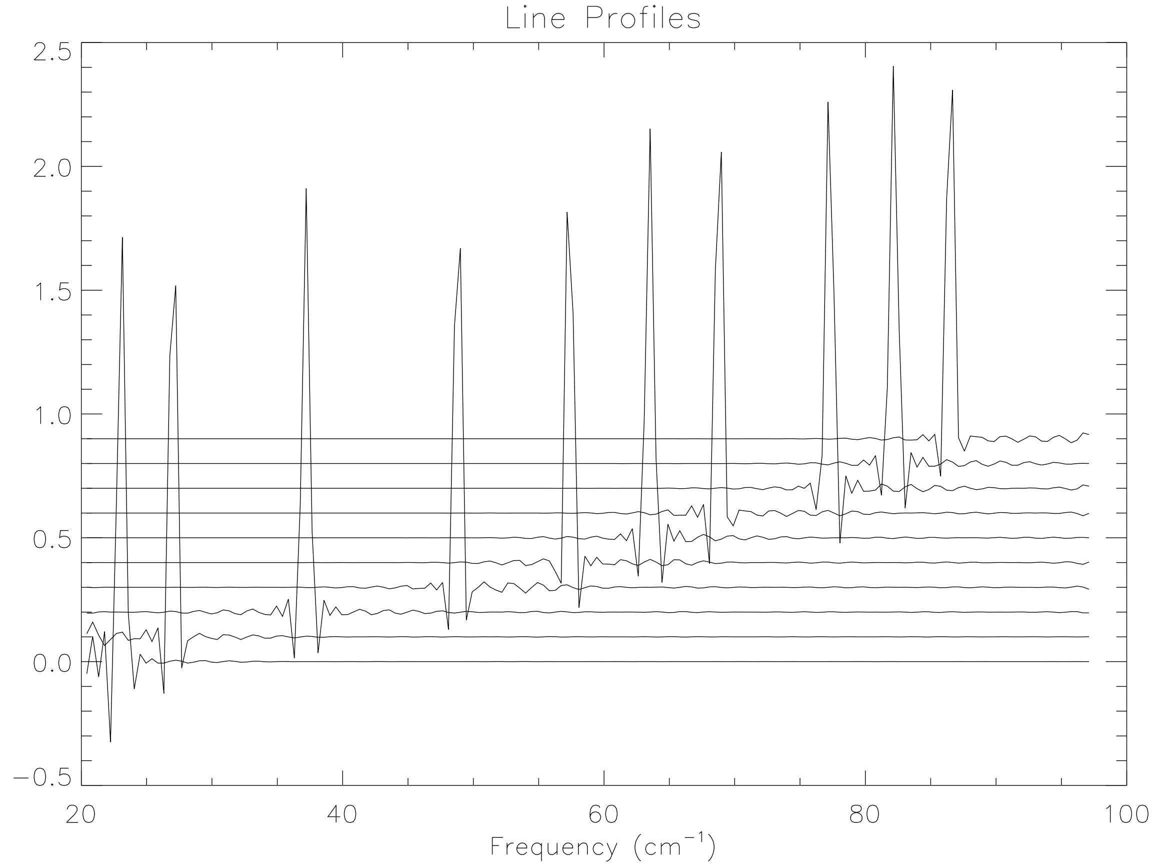

Fig. 8.6.— Model line profiles — For all lines fit in the HIGH data. Each line is offset 0.1 from the previous line for clarity.

spectrum diverges from that of the sky spectra. The synthetic spectrum is "calibrated" by multiplying the spectrum on a pointwise basis by the gain function, $G(\nu)$, described in Section 5.6 for the appropriate scan mode. The resulting calibrated synthetic line spectrum or line profile is

$$\zeta(\nu) \;=\; \Omega^{-1}G(\nu) \int_{-\infty}^{+\infty} dx\, \exp[2\pi i\nu x]\, A(x)\, I(x) \tag{47}$$

or

$$\zeta(\nu) \;=\; \Omega^{-1}G(\nu) \int_{-\infty}^{+\infty} dx\, \exp[2\pi i\nu x]\, A(x)\, \cos(2\pi\nu_L x)\, \exp[-\frac{1}{2}(\frac{\nu_L}{\nu_\circ}\frac{x}{\sigma})^2] \tag{48}$$

where $\zeta(\nu)$ is the line profile at the frequency ν, ν_L is the line frequency, Ω is a normalization factor, G is the gain function, and $A(x)$ is the apodization function.

The normalization is set so that the resulting profile in MJy sr^{-1} is for a line with incident surface brightness of one nW m^{-2} sr^{-1}. A detailed discussion of the *FIRAS* line profiles is given in Section 3 of the second *FIRAS* lines paper (Bennett *et al.* 1994), which is included as Appendix D. The delivered data sets include line profiles for each of the lines in Table 8.1. The line profiles for each low frequency channel and scan mode are contained in a single FITS file. Similarly, the line profiles for each high frequency channel and scan mode are contained in a single FITS file; the headers for these FITS files are given in Appendix G. The HIGH line profiles are plotted in Figure 8.3.

8.4.2. Modeling Spectral Lines

To determine maps of line intensity, we used data that has the zodiacal emission, the CMBR, and a model for the galactic dust removed. We fit the residual spectrum to a set of line intensities, F_m. We allow for residual continuum variations using a polynomial representation. So, we minimize for each pixel, p:

$$\chi_p^2 = \sum_\nu \left[S_{\nu p} - \sum_m F_{mp}\zeta_{m\nu} - \sum_k a_{kp}L_{k\nu} \right]^2 \frac{n_p}{C_\nu^2} \tag{49}$$

with respect to F_{mp} (the line fluxes) and the continuum residual coefficients a_{kp}, where $\zeta_{m\nu}$ are the line profiles, and $L_{k\nu}$ are the Legendre polynomials. The low frequency spectral fit uses a 4th order polynomial baseline, while the high frequency fit uses a 10th order baseline.

The line-subtracted continuum spectra are computed at each pixel using:

$$S_{\mathrm{line-sub};\nu p} = S_{\nu p} - \sum_m F_{mp}\zeta_{m\nu} \tag{50}$$

where F_{mp} are the line maps.

The *FIRAS* line emission and continuum spectrum maps are part of the data release. Their FITS headers are given in Appendix G.

The LOWF line emission skymap contains fluxes for eight low frequency lines, and the HIGH line emission skymap contains fluxes for ten high frequency lines The HIGH line emission skymap contains the fitted Galactic dust parameters. (Table 8.1). The uncertainties in the line fluxes and dust parameters are included in the line emission skymap records. These are formal uncertainties derived from the detector noise. In regions near the Galactic plane, the uncertainties introduced by the *FIRAS* gain uncertainties dominate (Section 7.2).

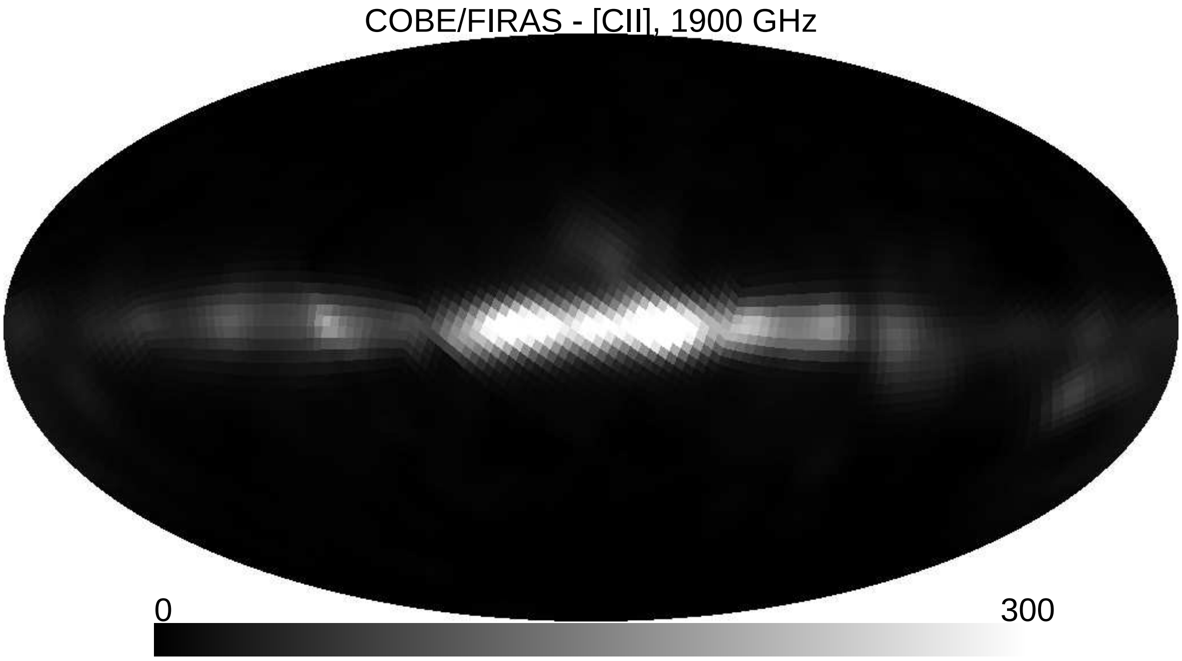

Fig. 8.7.— [CII] 1900 GHz flux map, linear stretch — (nWm^{-2}sr^{-1}). The strongest line detected by *FIRAS*. (qv. Figure 8.1)

Figures 8.7 and 8.8 map the [CII] 1900 GHz line flux. This is the strongest line detected by *FIRAS* (Bennett *et al.*, 1994a). Figure 8.6 maps the [NII] 1461 GHz line flux.

Figure 8.4 is a map of the fitted dust temperature. Figure 8.2 is a map of the dust emission normalization, τ. Figure 8.3 is a similar map on a log scale chosen to show the variation in the dust emission at higher Galactic latitudes.

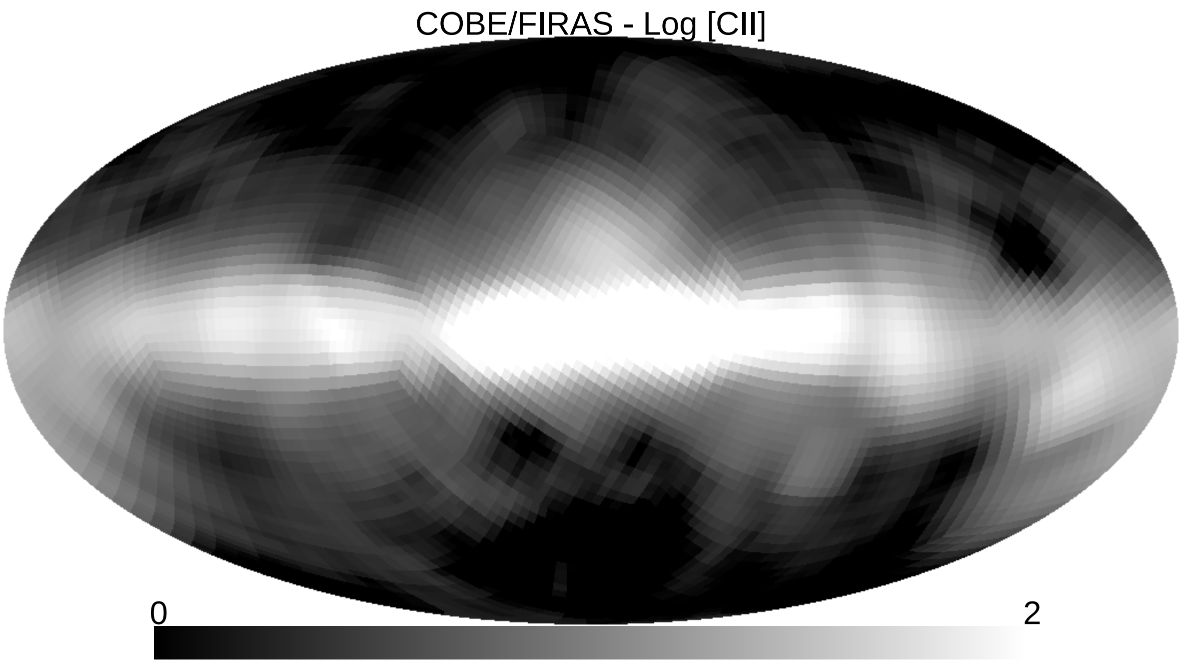

Fig. 8.8.— [CII] flux map, logarithmic stretch — (cf. Figure 8.7)

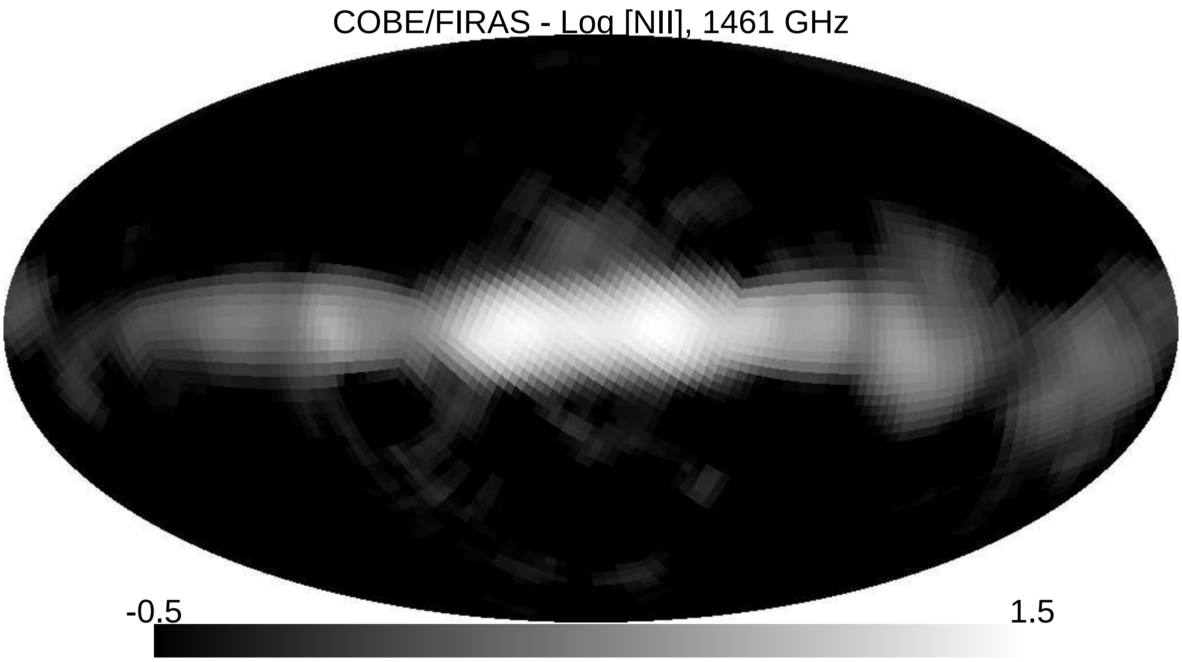

Fig. 8.9.— [NII] 1461 GHz flux map, logarithmic stretch — ($nWm^{-2}sr^{-1}$). Another strong emission line associated with warm ionized as well as neutral gas.